

Three case studies of height-time profiles of prominence eruptions observed by AIA and LASCO

Ts Tsvetkov*, N. Petrov

Institute of Astronomy and National Astronomical Observatory, Bulgarian Academy of Sciences, 72, Tsarigradsko Chaussee Blvd. 1784, Sofia, Bulgaria

ARTICLE INFO

Keywords:
Solar activity
Filaments
Eruptions
Oscillations
Coronal mass ejections (CMEs)

ABSTRACT

The motions of three solar eruptive prominences are studied. The behaviour of the rising prominence body during the eruption is tracked. Height-time profiles of the eruption up to $6 R_{\odot}$ (based on observations by Solar Dynamics Observatory/Atmospheric Imaging Assembly (HeII 304 Å) and Large Angle and Spectrometric Coronagraph Experiment (LASCO) C2/Solar and Heliospheric Observatory (SOHO)) and possible changes of the velocity of the prominence material are presented. The mechanisms that generate the variations in the material movement are discussed.

1. Introduction

Solar prominences are a spectacular manifestation of the solar activity. They are structures of dense, cool plasma ($n_e = 10^{10} - 10^{11} \text{ cm}^{-3}$ and $T = 10^4 \text{ K}$) surrounded by a hotter and rarefied coronal environment (in the corona: $n_e = 10^8 - 10^9 \text{ cm}^{-3}$ and $T = 10^6 \text{ K}$) (Tandberg-Hanssen, 1974, 1995). Bright in H_{α} emission when protruding from the limb, prominences appear darker than the surrounding chromosphere when seen on the disk, where they are referred to as filaments (McCauley et al., 2015). The terms prominence and filament are used interchangeably in the current article.

Since the beginning of the regular scientific observations various ways of dividing prominences in different groups and classes were proposed, but the most commonly used classification divides them in two groups - quiescent and active (Secchi, 1875). Quiescent prominences often arise at the base of coronal streamers (Engvold et al., 1990) and their existence may last from a few minutes to a few solar rotations. The life of active prominences is shorter (usually up to a few hours), but they are dynamical structures that show variations in shape and size. Often they emerge in active regions. Other parameters of prominences (mass density, degree of ionization, magnetic field strength, mean molecular weight, electron and gas pressures, etc.) are presented by Jensen and Wiik (1990).

During their existence prominences may undergo a process of destabilization and subsequent activation changes. The activation phase is a transition from nearly quiescent state to active one within few hours (Kilper et al., 2009). Typical rising velocities of the prominences during this stage are $1-10 \text{ km s}^{-1}$ (Sterling and Moore, 2004a,b). The structure of the filament, as well as its form, changes during activation - the

prominences become brighter and filaments - longer and darker. It may lead to an eruptive phase and transform the prominence into an eruptive one.

The beginning of the eruptive phase is the moment of rapid acceleration of the prominence on certain critical height. The eruption can be final or temporary phase of a quiescent prominence development. A prominence can lose a part of its material during the eruption. The amount of escaping material, its velocity and moving direction often depend on the surrounding magnetic structure and the balance of velocities in the different parts of the filament (Rompolt, 1997; Xia et al., 2014). The eruptive process is caused by eruption of the so-called Huge Magnetic System (HMS) described also by coronal cavity/prominence flux rope model (Berger, 2012). The colder and denser prominence material remains frozen-in the HMS during the eruption (Rompolt, 1984). According to the part of the HMS where the magnetic reconnection happens and the amount of filament mass that escapes the Sun, three different eruption types can be distinguished - full, partial or failed (Gilbert et al., 2007b). Early observations demonstrate that during the eruption the velocities of prominence plasma reach over 700 km s^{-1} (Ball, 1906). However, recent studies claim that velocities may increase from a few to 400 km s^{-1} , according to Gopalswamy et al. (2003), 100 km s^{-1} up to over 1000 km s^{-1} (Schrijver et al., 2008) or $10-100 \text{ km s}^{-1}$ as generalized by Hurlburt (2015).

Rompolt (1990) uses the typology of the magnetic fields that support the filament to give another classification of the eruptive prominences (EPs), distinguishing two types of EPs. Type I are symmetric, archwise EPs with legs, anchored in the solar surface. During the eruption the arch rises and expands and remains visible in H_{α} spectral line until the end of the eruptive process. Type II are asymmetric EPs. At

* Corresponding author.

E-mail address: tstsvetkov@astro.bas.bg (T. Tsvetkov).

Table 1
Basic data for the explored prominences.

	EP I	EP II	EP III
Date and Time [UT]	2011 June 6 03:30–12:00	2012 July 28/29 15:30–03:30	2013 February 27 00:00–07:30
First Appearance [UT]	2011 June 1 01:00	2012 July 27 01:00	2013 February 25 00:00
Position	SW limb	SE limb	SW limb
Association with ARs	No	No	No
Association with CMEs	Yes	Yes	Yes
Association with flares	No	No	No
Association with SEP fluxes	No	No	Yes
Eruption type	Partial	Full?	Full
Symmetry	Symmetric	Symmetric?	Symmetric
Direction of propagation	Radial	Radial	Radial
Twist	No	Yes	Yes

first, their shape is very similar to Type I, but in the very beginning of the eruption, one of the legs of the prominence body often breaks away and rises until it becomes almost perpendicular to the solar surface. Type II EPs usually show post-eruptive phase when the prominence material falls down to the chromosphere.

The current study presents our first attempt to investigate possible variations of solar prominences velocity, which appear on the height-time diagrams of the eruptions. Although different authors explored different kind of oscillations of the Sun (Williams et al., 2001; Schmieder et al., 2017), the idea for velocity alterations of eruptive prominences presented here has never been considered.

2. Observations

The current study utilizes space-based observations and presents three case studies of solar prominences, observed by the Atmospheric Imaging Assembly (AIA; Lemen et al., 2012) aboard the Solar Dynamics Observatory (SDO; Pesnell et al., 2012). We analysed HeII 304 Å channel images, taken with an average cadence of about 5 min. The data from the Large Angle and Spectrometric Coronagraph Experiment (LASCO)/Solar and Heliospheric Observatory (SOHO) showed not only possible association of the EPs with coronal mass ejections (CMEs), but also allowed us to observe the prominence material in the core of the CME on higher altitudes (covering the distance range of 1.5–6 R_{\odot} (solar radii); cadence - 12–15 min).

Three eruptive prominences located above the solar limb (two on the southwestern (SW) side and one on the southeastern (SE)) are presented, which allows their tracking as far away from the limb as possible. These directions (same as northeastern (NE) and northwestern (NW)) offer the longest series of measurements. On the other hand, the filaments are observed in 3 different years to exclude the possibility to be connected with identical active processes. Some basic information for the explored prominences is summarized in Table 1. The data for the possible association with active regions is based on the provided information by <https://solarmonitor.org>. The associations with CMEs, flares and solar energetic particle (SEP) fluxes are defined by the following catalogues: SOHO LASCO CME Catalog¹ (Yashiro et al., 2004; Gopalswamy et al., 2009), Wind/WAVES Database² and Wind/EPACT proton event catalogue.³ The source of the information about the eruption type, the symmetry, direction of propagation and the twist, where available, is the AIA Filament Eruption Catalog,⁴ created by McCauley et al. (2015). The reason for the ambiguous data about the

eruption type and symmetry of EP II is the two-dimensional projection of the EPs only observed in 304 Å channel by the authors of the catalog.

2.1. EP I

The first prominence from 2011 June 6 erupted on the SW limb between 03:30 and 12:00 UT (in AIA/SDO and LASCO C2 field of views - FOVs) on heliographic latitude $\approx 70^{\circ}$ S at mean position angle $\approx 240^{\circ}$ (Fig. 1). The eruption was symmetric (type I) and partial.

It was associated with a CME that appeared at 07:30 at central position angle $\approx 241^{\circ}$, moving with linear speed about 582 kms^{-1} . In the LASCO C2 FOV also the EP on higher altitudes could be observed (Fig. 2).

2.2. EP II

Between 15:30 UT on 2012 July 28 and 03:30 UT on 2012 July 29 (visible from both AIA and LASCO observations) an eruption occurred on the SE limb (mean latitude $\approx 20^{\circ}$ S) (Fig. 3). The EP was neither associated with active region, nor with a flare. SEP flux was not detected.

The associated CME from 23:48 UT on 2012 July 28 at central position angle $\approx 136^{\circ}$ moved with linear speed about 460 kms^{-1} , carrying the filament at its core (Fig. 4).

2.3. EP III

The third observed EP (2013 February 27, 00:00–07:30 UT - AIA and LASCO C2) appeared on $\approx 45^{\circ}$ S, mean position angle $\approx 260^{\circ}$ (Fig. 5). The EP was later seen in the LASCO C2 coronagraph FOV (Fig. 6) at the base of a partial halo CME. In LASCO C2 FOV the EP and the CME were the fastest among the presented here cases with velocities of 352 kms^{-1} and 622 kms^{-1} , respectively.

3. Measurements

3.1. Procedure

For data analysis we used procedures, included in IDL-based product – SolarSoftware (Bentley and Freeland, 1998). The primary data processing includes removing the bad pixels, subtracting the thermal noise, dividing by the flat fields, despiking and solar rotation correction. Measuring the kinematic characteristics of EPs requires defining the exact position of the highest part of the loop top above the solar limb on every frame and tracking its change in time. While tracking the highest point of every prominence we measure not only the signal from the filament's top, but also the average background signal. Then we use the empirical rule stating that an event is considered to be practically impossible if it lies in the region of values of the normal distribution of a random variable at a distance from its mathematical expectation of more than three times the standard deviation. To emphasize the weak emission of some parts of the prominence we used color inverted images.

We used the information for the height of the filament and the time of registration of the images to plot a height-time diagrams of the eruptions.

3.2. Kinematics

The first appearance of the EP I happened on 2011 June 1 around 1:00 UT as a quiescent prominence on the SW limb (Table 1). After a probable magnetic reconnection, approximately 5 days later, it erupted ejecting the most of its matter into the heliosphere. Measuring the height of the prominence during the eruption allowed us to build a height-time diagram (Fig. 7) and to track its behaviour while rising from 130 000 km to 385 000 km in the AIA FOV. The eruption

¹ https://cdaw.gsfc.nasa.gov/CME_list/.

² https://cdaw.gsfc.nasa.gov/CME_list/radio/waves_type2.html.

³ <http://www.stil.bas.bg/SEPcatalog/>.

⁴ <http://aia.cfa.harvard.edu/filament/>.

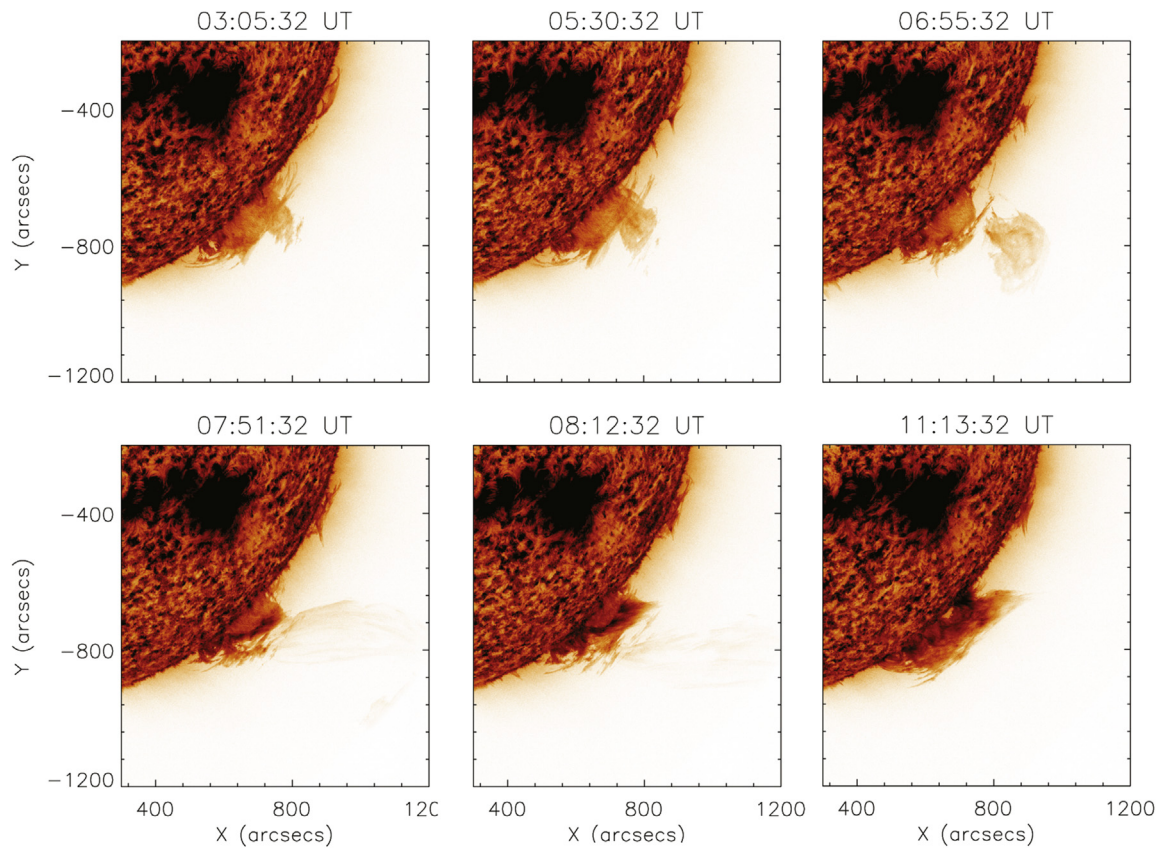


Fig. 1. Beginning of the eruptive phase of the prominence, observed on 2011 June 6. The images are obtained in the He II 304 Å channel of AIA/SDO.

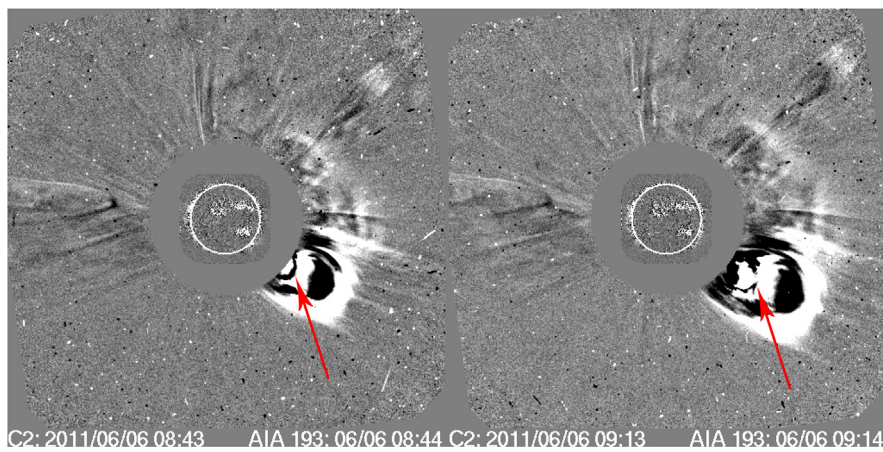


Fig. 2. The EP from 2011 June 6 (marked with arrows) as a core of a CME in LASCO C2 FOV.

continued and the prominence became a core of a CME, visible in LASCO C2 FOV, rising up to $\approx 3.385 \times 10^6$ km ($\lesssim 4.9 R_{\odot}$). We measured the average rising velocity above 250 000 km until the filament disappears in AIA FOV to be $\approx 36 \text{ kms}^{-1}$ reaching up to $\approx 289 \text{ kms}^{-1}$ in C2 FOV.

The EP II from 2012 July 28/29 showed similar behaviour, even

though it came into view on the SE limb only a day before the partial eruption started (Table 1). At the very beginning of the measurements its highest part was ≈ 120 000 km above the limb, reaching ≈ 380 000 km before hiding from the FOV of AIA (Fig. 8) rising with average velocity of $\approx 21 \text{ kms}^{-1}$. At the final moments of visibility in LASCO C2 FOV (12 h after the start of the eruption) the outer segments

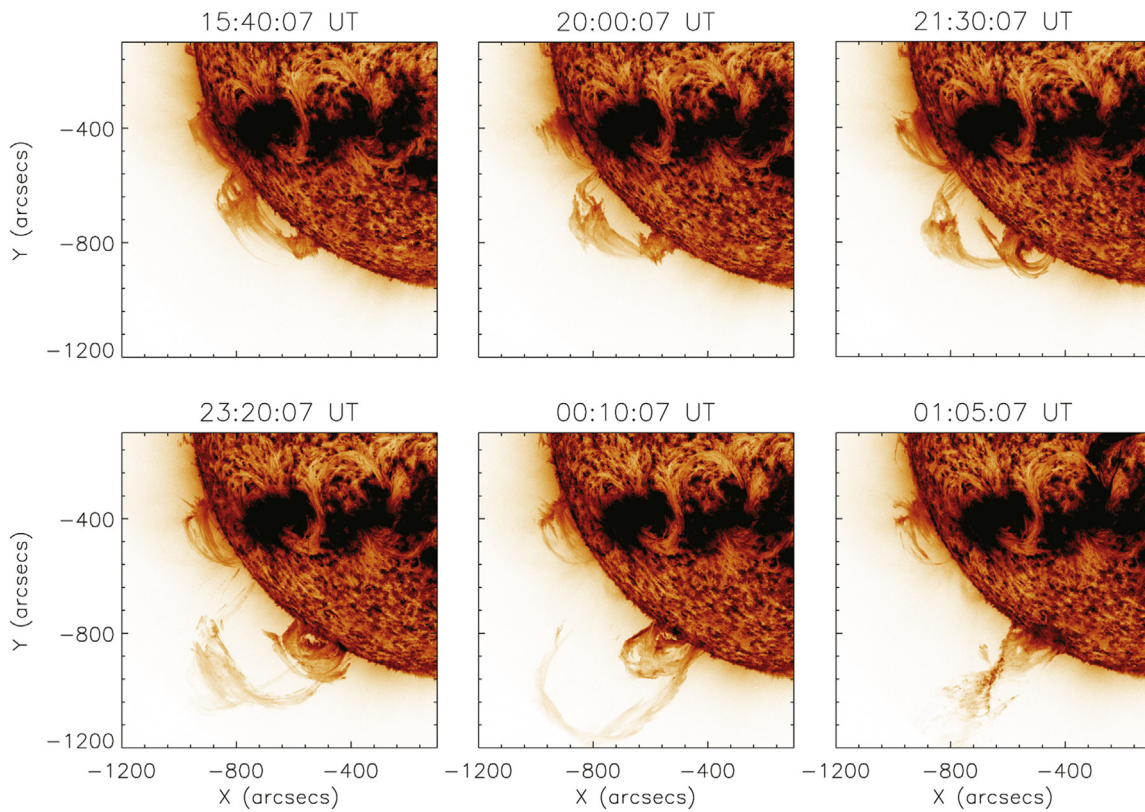


Fig. 3. The eruption of the prominence from 2012 July 28/29, captured by AIA/SDO (He II 304 Å).

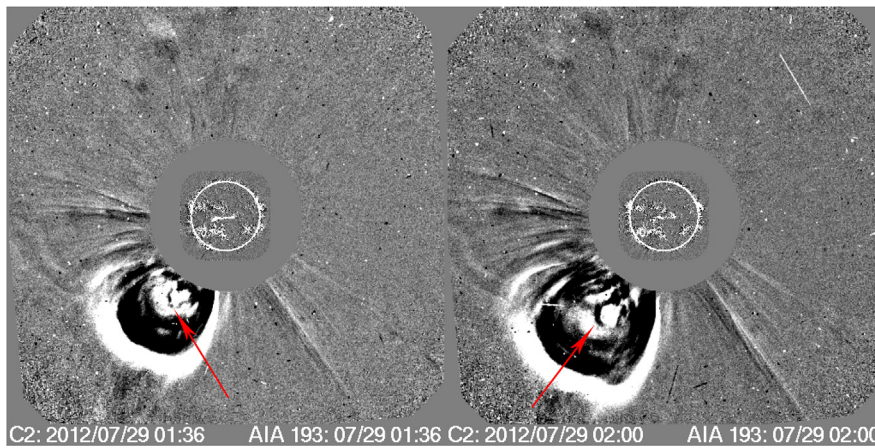


Fig. 4. LASCO C2 images from the appearance and rising of the prominence on 2012 July 29 (marked with arrows).

of the prominence material were $\approx 2.970 \times 10^6$ km ($\approx 4.3 R_{\odot}$) away from the solar limb. The average velocity of the movement observed by LASCO was ≈ 278 km s $^{-1}$, which makes the eruption from 2012 July 28/29 the slowest of the explored ones.

The EP III (2013 February 27) erupted quickly after showing up (2 days later) on the SW limb. Its activation led to ejection of large amount of prominence matter, which defined the full eruption type (Table 1).

The 7-h long eruption (00:00–07:00) was relatively slow. The maximal heights reached in the two instruments are ≈ 275 000 km with average velocity at the final stages of visibility of ≈ 32 km s $^{-1}$ (AIA) and $\approx 3.8 R_{\odot}$ reaching ≈ 352 km s $^{-1}$ before disappearing in C2 FOV (Fig. 9).

The LASCO C2 observations start above $1.5 R_{\odot}$ and every prominence leaves the AIA FOV on different height depending on their morphology, the angle between the main axis of the prominence and

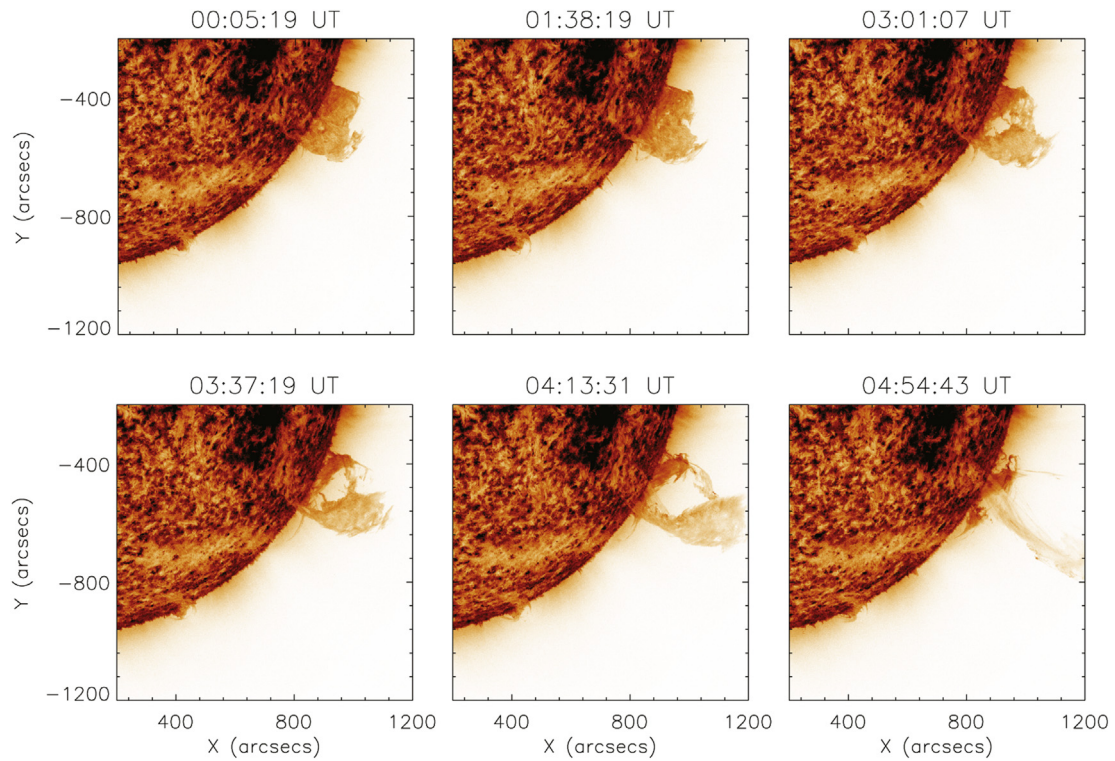


Fig. 5. The eruptive phase of the prominence observed on 2013 February 27. The images are obtained in the He II 304 Å channel of AIA/SDO.

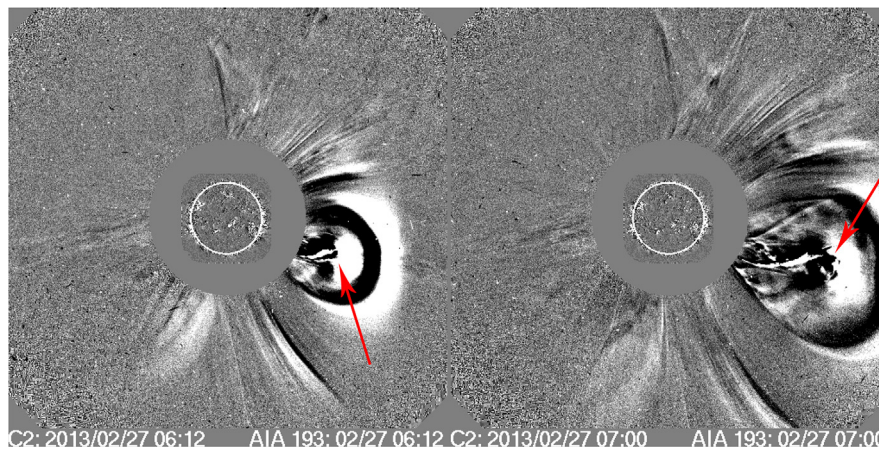


Fig. 6. LASCO C2 images of the EP III (marked with arrows) at the base of a CME registered between 6:12 UT and 7:00 UT on 2013 February 27.

solar limb, etc. The time in between determines the gaps on Figs. 7a, 8a and 9a. The size of the gap is also fixed by the velocity of the eruptive prominence.

In all of the cases presented in the current study we see EPs reaching heights in the range between 250×10^3 and 400×10^3 km in AIA FOV and 3.5 to $5 R_{\odot}$ seen from LASCO C2 coronagraph. Summary of the results are presented in Table 2. The duration of measurements in the relevant instrument is marked as Δt . The maximal height reached in the

FOV of the respective instrument is denoted as h_{max} . We measure only average velocities above $250\,000$ km to present typical velocities for the eruptive phase (v). Calculated velocities coincide well with defined from Gopalswamy et al. (2003), Schrijver et al. (2008) and Hurlburt (2015) – see Section 1.

In the height-time profiles of the presented cases two typical stages of the eruption are noticeable: activation and eruption phase. We reckon that the behaviour of prominence plasma observed on height-

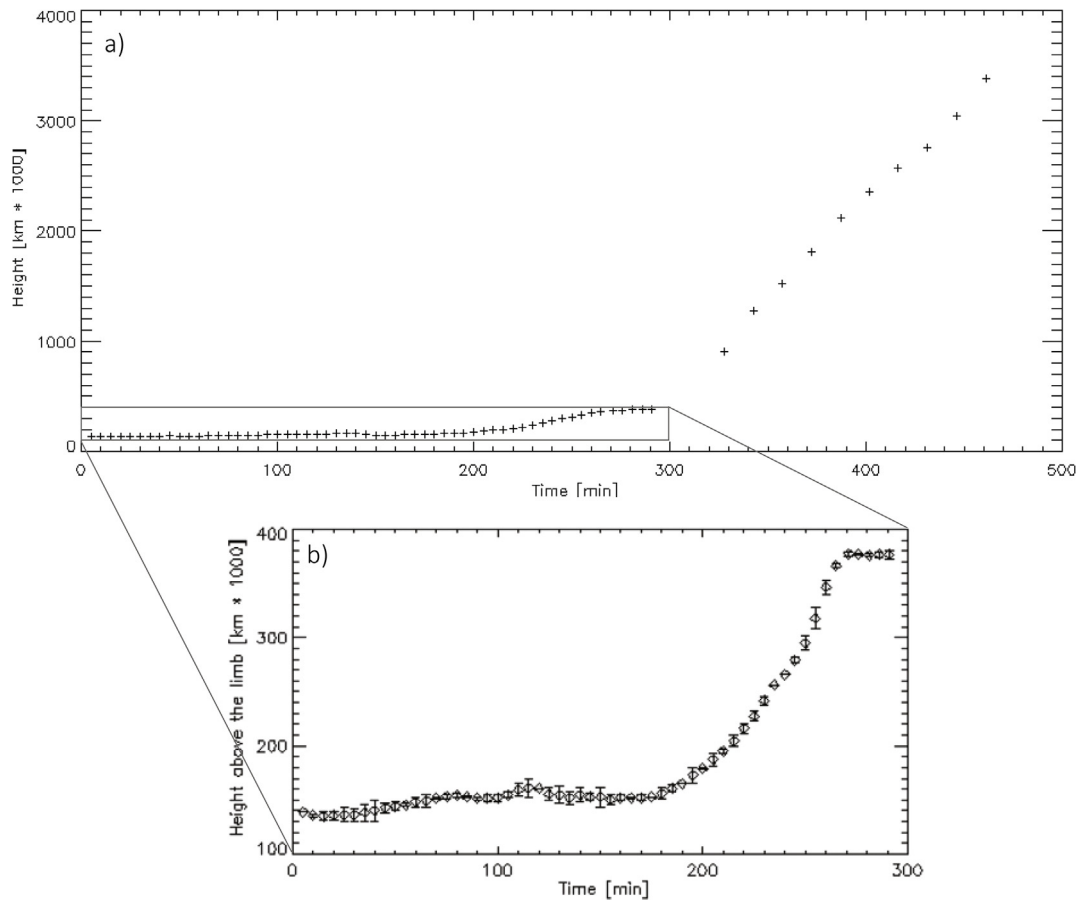


Fig. 7. Height-time profiles of the prominence on 2011 June 6. The onset time is 03:00 UT. a) Including measurements from SDO/AIA and SOHO/LASCO C2. b) A zoom-in of the AIA/SDO 304 Å data. By the symbol + are presented our measurements. The continuous line is a spline fit of the measurements that present the changes in speed of the plasma raising in the solar corona.

time profiles are connected to its supporting magnetic configuration. The beginning of the eruptive phase marks the onset of large-scale magnetic reconnection (Joshi et al., 2016). This stage could be connected to the passage of prominence material through coronal cavities accompanied by velocity increase up to $20\text{--}40\text{ km s}^{-1}$. The observed flattening of the leading edge of prominence body traces the boundaries of the helical magnetic flux rope, defined by Berger (2012) as a structure in the solar corona that consists of prominences and coronal cavities. Usually, coronal structures are visible in white-light observations above solar prominences during total solar eclipses or in EUV SDO/AIA 211 Å channel. Images showing the environment of the explored filaments in the last moments of activation and before the onset of the eruptive phase are presented on Fig. 10. To increase their contrast, we used image differences between the original AIA image and its smoothed version. On Fig. 10 (left and right) loops-like structures and cavities surrounding the EPs from 2011 June 6 and 2013 February 27 are distinguishable (enclosed in rectangles). Coronal cavities are dark due to a $\sim 30\text{--}40\%$ density deficit relative to the surrounding arcade (Vázquez et al., 2009; Fuller and Gibson, 2009). The presence of coronal cavities is important because they form the bulk of quiet-Sun CMEs, accounting for 40% of all solar eruptions (Gopalswamy, 2006; Pevtsov et al., 2012). Around the EP from 2012 July 28 (Fig. 10 middle) coronal

structures are harder to notice probably because of projection effects of superposition of structures from EP magnetic field and the nearby active region 11 532. Gibson et al. (2010) explain observations of prominences without associated coronal cavities as line-of-sight effects in which the cavity is occluded by foreground arcade emission. The increment of velocity continues above coronal cavities in open coronal structures observed by SOHO/LASCO C2. Similar effects are harder to notice during filament eruptions on solar disk. We also inspected AIA 193 Å data and did not find a coronal holes nearby any of the EPs.

These three case studies are used as a starting point for testing the hypothesis that filament plasma passage through separate magnetic field arcade structures could give rise to temporary delays. The process of weak magnetic reconnection or the interaction of EPs with the surrounding magnetic environment could be indicated as possible reason. Passing through the open radial fields at altitudes higher than $2\text{--}2.5 R_{\odot}$ (Fisk, 2005; Gilbert et al., 2007a), the mass reaches a height with free acceleration without oscillations.

4. Conclusions and discussions

The velocity distribution of the plasma in height during prominence eruption shows variations. They should not be considered as

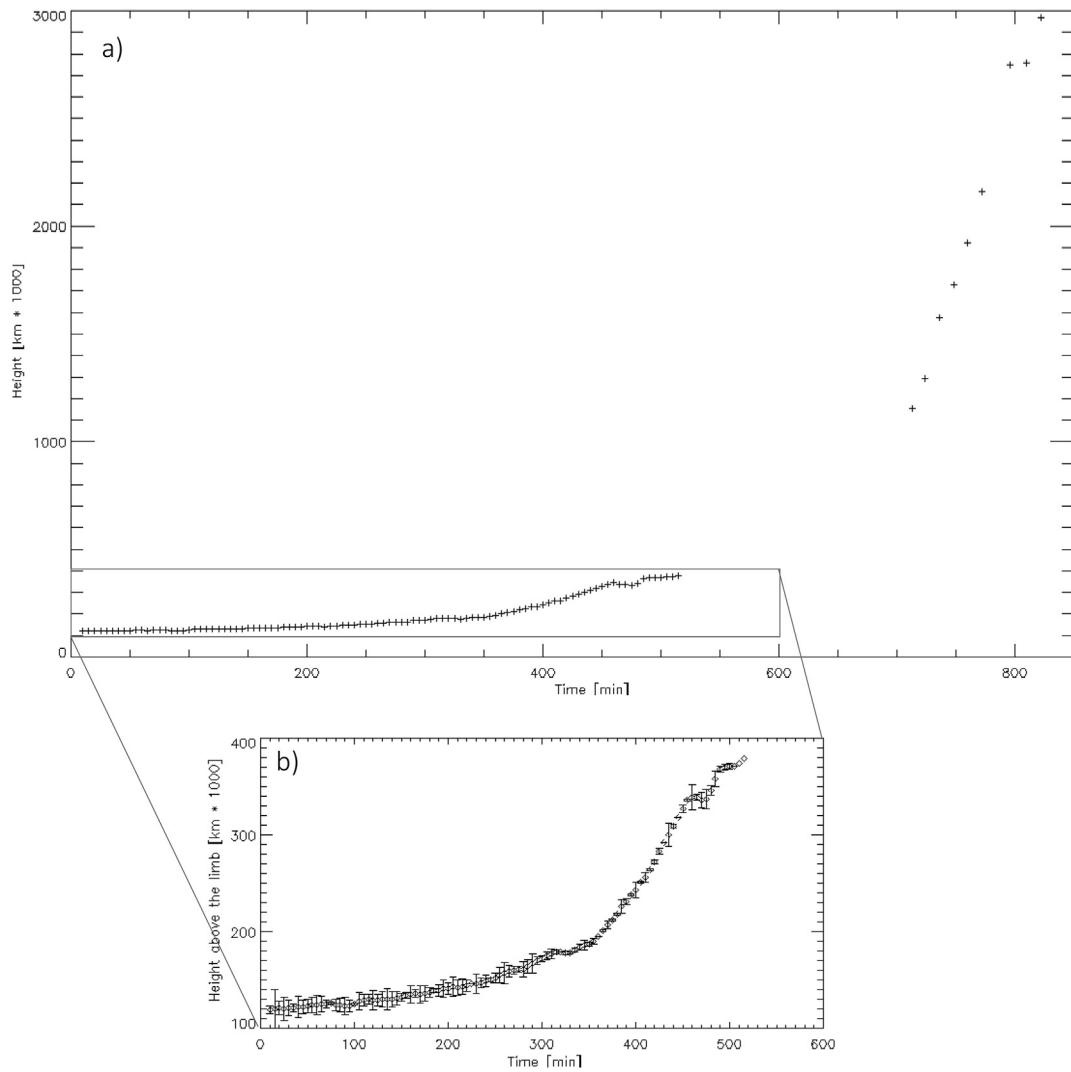


Fig. 8. Height-time profiles of the prominence on 2012 July 28/29. The onset time is 15:30 UT. a) Including measurements from SDO/AIA and SOHO/LASCO C2. b) A zoom-in of the AIA/SDO 304 Å data. By the symbol + are presented our measurements. The continuous line is a spline fit of the measurements that present the changes in speed of the plasma raising in the solar corona.

propagating waves or moving nodes in the meaning of MHD oscillation modes. We assume that the observed oscillations are due to magnetic loops overpassed by the prominence material. The surrounding magnetic structure of the filament defines its kinematics. When the plasma passes a single magnetic loop, the movement of the eruptive prominence slows down and its leading edge flattens, which may be considered as a consequence of interaction between prominence material and its surroundings.

According to the mass and the energy of the eruptive filament it is possible to observe an eruption when the plasma can completely pass over the surrounding magnetic loops or reach certain height above the

solar limb and flow back down to the Sun.

The variations are not visible in LASCO C2 data. It may be because of the slow cadance in LASCO/SOHO observations (12–15 min) or because a certain height of about 400 000 km above the solar limb is critical and the velocity of the EPs rapidly raises and velocity oscillations stop probably due to the lack of strong magnetic structures that can resist the free movement of material. Still, it can be connected to the low density of the corona, which cannot affect the velocity of the prominence plasma.

The current study contains only the very first results of our investigation. Its aim is to present some observational facts for the rising

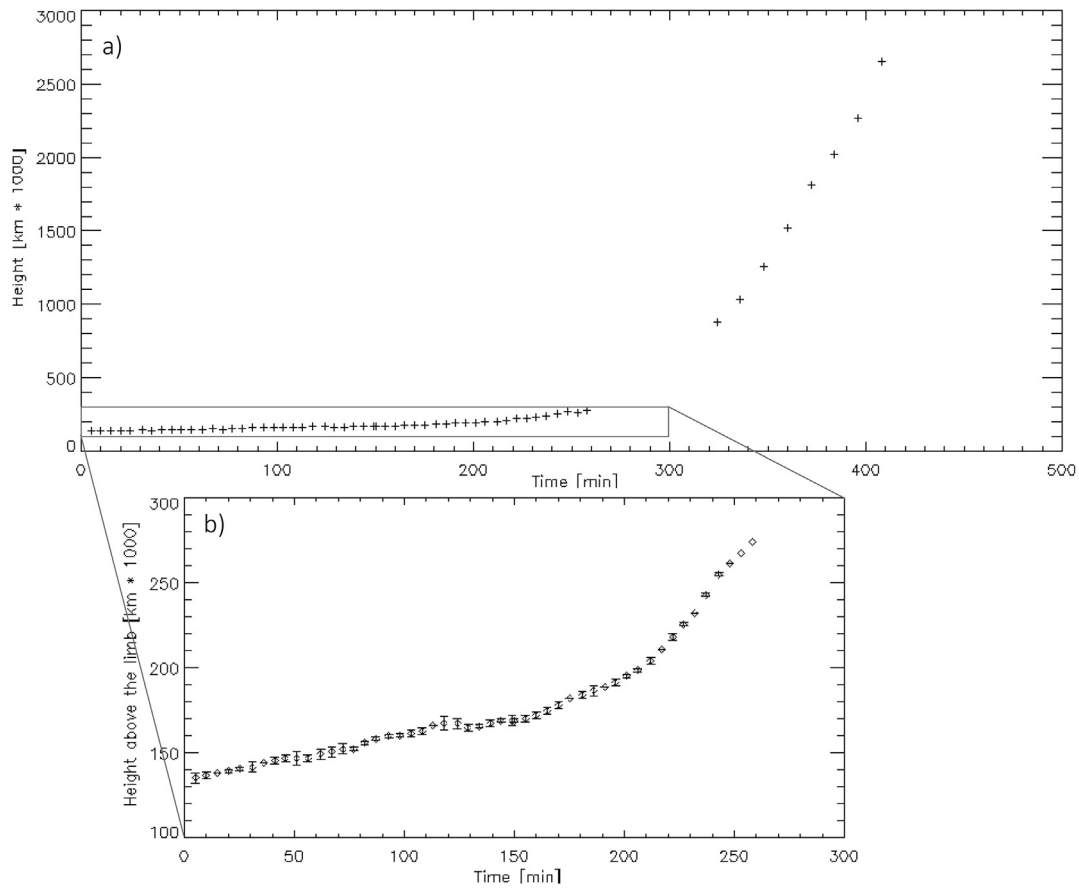


Fig. 9. Height-time profiles of the prominence on 2013 February 27. The onset time is 00:00 UT. a) Including measurements from SDO/AIA and SOHO/LASCO C2. b) A zoom-in of the AIA/SDO 304 Å data. By the symbol + are presented our measurements. The continuous line is a spline fit of the measurements that present the changes in speed of the plasma raising in the solar corona.

Table 2

Kinematics of the explored prominences in AIA and LASCO C2 FOVs. Denoted as Δt are the durations of observations, h_{max} – the largest height reached by the rising prominence arch in the FOV of the respective telescope, v – average velocity of the rising filament above 250 000 km and v_{CME} – the linear speed of the associated CME as measured in SOHO LASCO CME Catalog.

AIA			LASCO C2				
Δt	h_{max}	v	Δt	h_{max}	v	v_{CME}	
[min]	[km]	[kms ⁻¹]	[min]	[km (R_{\odot})]	[kms ⁻¹]	[kms ⁻¹]	
EP I	291	385 000	36	133	3.385×10^6 (4.9)	289	582
EP II	513	380 000	21	112	2.970×10^6 (4.3)	278	460
EP III	249	275 000	32	84	2.652×10^6 (3.8)	352	622

of the eruptive prominences. Subsequent papers will explore larger amount of data to confirm or to disprove the hypotheses for the observed variations. Future steps include exploring the origin of the velocity variations in the height-time profiles.

Acknowledgement

This work was supported by National Science Fund of Bulgaria with grant DN 08-1/2016, contract No. DNTS/Russia 01/6 (23-Jun-2017) and the joint projects of cooperation between the IA NAO, BAS, and Astronomical Institute of Wroclaw University, PAN, and the Department of Astronomy, Faculty of Mathematics, University of Belgrade, Serbia.

The used CME catalog is generated and maintained at the CDAW Data Center by NASA and The Catholic University of America in cooperation with the Naval Research Laboratory. SOHO is a project of international cooperation between ESA and NASA.

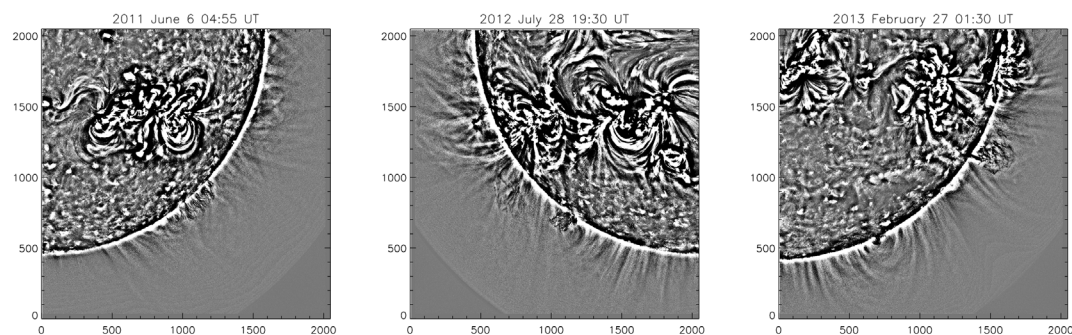


Fig. 10. AIA 211 Å channel image differences for EP I (left) - 2011 June 6 04:55 UT, EP II (middle) - 2012 July 28 19:30 UT and EP III (right) - 2013 February 27 01:30 UT. With rectangles are marked archwise structures and coronal cavities that surround EPI and EPIII, while the surroundings of EPII are hard to distinguish because of overlay with the magnetic field lines of the nearby active region. The units on both axes are given in pixels as $1 \text{ px} \approx 442 \text{ km}$ on left and middle images and $1 \text{ px} \approx 431 \text{ km}$ on the right image.

Appendix A. Supplementary data

Supplementary data related to this article can be found at <http://dx.doi.org/10.1016/j.jastp.2018.05.013>.

References

- Ball, R.S., 1906. The story of the Sun. Cassell and Company Ltd, London, Paris, New York and Melbourne, pp. 186.
- Bentley, R.D., Freeland, S.L., 1998. In: Crossroads for European Solar and Heliospheric Physics, Recent Achievements and Future Mission Possibilities, vol. 417. ESA Spec. Publ., pp. 225.
- Berger, T., 2012. In: Rimmele, T.R., Collados Vera, M. (Eds.), ASP Conference Series. vol. 463.
- Engvold, O., Hirayama, T., Leroy, J., et al., 1990. In: Ruzdjak, V., Tandberg-Hanssen, E. (Eds.), In Dynamics of Quiescent Prominences. vol. 117. I.A.U. Colloquium, pp. 294.
- Fisk, L.A., 2005. APJ (Acta Pathol. Jpn.) 626, 563.
- Fuller, J., Gibson, S.E., 2009. APJ (Acta Pathol. Jpn.) 700, 1205.
- Gibson, S.E., Kucera, T.A., Rastawicki, D., et al., 2010. APJ (Acta Pathol. Jpn.) 724 (2), 1133.
- Gilbert, H.R., Alexander, D., Liu, R., 2007a. Sol. Phys. 245, 287.
- Gilbert, J.A., Zurbuchen, T.H., Fisk, L.A., 2007b. APJ (Acta Pathol. Jpn.) 663, 583.
- Gopalswamy, N., 2006. JApA 27, 243.
- Gopalswamy, N., Shimojo, M., Lu, W., et al., 2003. APJ (Acta Pathol. Jpn.) 586, 562.
- Gopalswamy, N., Yashiro, S., Michalek, G., et al., 2009. Earth Moon Planets 104, 295.
- Hurlburt, N., 2015. J. Space Weather Space Clim 5, A39.
- Jensen, E., Wiik, J.E., 1990. In: Ruzdjak, V., Tandberg-Hanssen, E. (Eds.), Dynamics of Quiescent Prominences, IAU Coll. 117, Lecture Notes in Physics 363, pp. 298.
- Joshi, B., Kushwaha, U., Veronig, A.M., Cho, K.-S., 2016. APJ (Acta Pathol. Jpn.) 832 (2), 130.
- Kilper, G., Gilbert, H., Alexander, D., 2009. APJ (Acta Pathol. Jpn.) 704, 522.
- Lemen, J.R., Title, A.M., Akin, D.J., et al., 2012. Sol. Phys. 275, 17.
- McCaughey, P.L., Su, Y., Schanche, N., et al., 2015. Sol. Phys. 290, 6.
- Pesnell, W.D., Thompson, B.J., Chamberlin, P.C., 2012. Sol. Phys. 275, 3.
- Pevtsov, A.A., Panasenco, O., Martin, S.F., 2012. Sol. Phys. 277, 185.
- Rompolt, B., 1984. Adv. Space Res. 4 (4), 357.
- Rompolt, B., 1990. Hvar. Obs. Bull. 14 (1), 37.
- Rompolt, B., 1997. Material Ejection from the Sun-i, Cracow, Poland.
- Secchi, A., 1875. Le Soleil, vols. 1 and 2 Gauthier-Villars, Paris.
- Schmieder, B., Peter, L., Labrosse, N., et al., 2017. American Astronomical Society, SPD Meeting No. 48.
- Schrijver, C.J., Elmore, C., Kliem, B., Török, T., Title, A.M., 2008. APJ (Acta Pathol. Jpn.) 674, 586.
- Sterling, A.C., Moore, R.L., 2004a. APJ (Acta Pathol. Jpn.) 602, 1024.
- Sterling, A.C., Moore, R.L., 2004b. APJ (Acta Pathol. Jpn.) 613, 1221.
- Tandberg-Hanssen, E., 1974. Solar Prominences. D. Reidel Publ. Co., Dordrecht, Holland, pp. 169 (GAM 12).
- Tandberg-Hanssen, E., 1995. The Nature of Solar Prominences. vol. 199 Ap&SS Library, Dordrecht, Holland.
- Vásquez, A.M., Frazin, R.A., Kamalabadi, F., 2009. Sol. Phys. 256, 73.
- Williams, D.R., Phillips, K.J.H., Rudawy, P., et al., 2001. Mon. Not. Roy. Astron. Soc. 326, 428.
- Xia, C., Keppens, R., Guo, Y., 2014. APJ (Acta Pathol. Jpn.) 780, 130.
- Yashiro, S., Gopalswamy, N., Michalek, G., et al., 2004. JGR 109, A7.